THE JOURNAL OF PHYSICAL CHEMISTRY B

Article

pubs.acs.org/JPCB

Oriented Electrophoretic Deposition of GdOCl Nanoplatelets

Kenneth R. Kort and Sarbajit Banerjee*

Department of Chemistry, University at Buffalo, The State University of New York, Buffalo, New York, 14260, United States

ABSTRACT: Electrophoretic deposition has emerged as a versatile and precisely tunable approach for the rapid deposition of conformal thin films of colloidal nanocrystals. The electrophoretic deposition of phosphor particles has assumed special significance in recent years as a commercially viable means toward the fabrication of large-area, ultrathin high-resolution emissive display screens. Here, we demonstrate that the anisotropic shape of colloidal ligand-passivated GdOCl nanoplatelets enables their assembly with remarkable substrate alignment and a high packing density upon electrophoretic deposition. GdOCl nanocrystals are promising candidates for phosphor applications given their low maximum phonon cutoff energy, robust chemical stability over prolonged periods of operation, and ability to promote efficacious phonon energy transfer to dopant ions. Potentiostatic deposition of GdOCl nanoplatelets from cyclohexane dispersions allows the deposition of individual nanoplatelets with their basal planes parallel to the electrode surface. Tuning the applied voltage and solution concentration allows control of film thickness, ranging up to several tens of micrometers. The high degree of particle alignment is attributed to anisotropic charge distribution and entrainment within electroosmotic flows established in the vicinity of the electrode surface. The oriented high-particle-density GdOCl nanoplatelet thin films are possible candidates for phosphor applications, which is illustrated by the green emission from a Tb-doped GdOCl thin film on indium tin oxide (ITO)-coated glass.

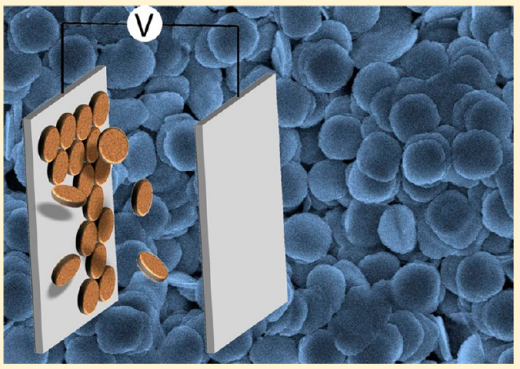

1. INTRODUCTION

The dimensional confinement of solid-state materials induces many remarkable properties, such as most famously, the plasmon resonance of noble metals, size-tunable bandgap emission of semiconductor quantum dots, superparamagnetic behavior of iron oxides, and the mechanical robustness of Mg alloys. Technological realization of the potential of nanoscience is predicated on assembling nanomaterials into macroscopic objects while still preserving the finite size of the nanoscopic constituent particles. Considerable attention has thus focused on nanomaterial assembly techniques such as Langmuir–Blodgett casting, layer-by-layer (LbL) deposition, evaporation-induced self-assembly, electrophoretic deposition, and field-assisted sintering.[1−9] When performed with an adequate extent of control, nanomaterial assembly techniques can yield constructs exhibiting novel emergent phenomena and enable precise patterning and positioning of nanomaterials in three-dimensional space. Electrophoretic deposition stands out among these methods as an entirely scalable, rapid, and conformal means to obtain nanoparticle coatings or near-net-shape objects with a high packing density.[10−16] In the context of assembling colloidal nanoparticles, electrophoretic deposition offers a far superior deposition rate as compared to self-assembly or Langmuir–Blodgett methods and further does not require the addition of any binders or additives (such as the polyelectrolytes typically used for LbL assembly).

The electrophoretic deposition of particles with nanoscale dimensions assumes special significance for the construction of phosphor thin films such as for flat panel emissive display and solid-state lighting applications.[17−21] Micrometer-sized phosphor particles are plagued by internal absorption losses and multiple scattering of emitted light. Substantial improvements in display quality can thus be engineered by scaling the constituent phosphor particles to nanoscale dimensions to mitigate the deleterious particle-mass-dependent effects of scattering.[22] High-resolution displays further require a high packing density of nanoscale particles with homogeneous pinhole-free coverage and low film thicknesses and consequently represent a particularly worthwhile target for fabrication by electrophoretic deposition.[21] Here, we present a potentiostatic approach for the electrophoretic deposition of colloidal GdOCl phosphor nanoplatelets from a nonpolar solvent. A high degree of substrate alignment of the constituent nanoplatelets is achieved within the deposited thin films, and macroscopic free-standing constructs of highly oriented nanoparticles can further be delaminated from the substrate.

Similar to oxyhalides of other early lanthanides, GdOCl is characterized by a low phonon cutoff energy.[23−26] In conjunction with its high chemical stability and effectual phonon energy transfer to dopant species, the low phonon cutoff threshold makes GdOCl well-suited for use as the host matrix of phosphor displays upon doping with the appropriate rare-earth dopant.[26−28] In recent work, we have reported a

Special Issue: Electrophoretic Deposition

Received: May 25, 2012
Revised: August 7, 2012
Published: September 10, 2012

   dx.doi.org/10.1021/jp3051142 | J. Phys. Chem. B 2013, 117, 1585–1591

nonhydrolytic sol−gel condensation route for the synthesis of well-defined GdOCl nanosheets and nanoplatelets in coordinating solvents and have demonstrated the upconversion of near-infrared illumination to green and red emission by Er-doped GdOCl nanocrystals.[23] Here, we demonstrate green emission from a thin film of Tb^{3+}-doped GdOCl nanoplatelets obtained with a high packing density of the primary particles. For technological implementation within displays, it is imperative to develop scalable high-throughput routes to integrate solution-synthesized GdOCl nanocrystals within thin-film architectures. To the best of our knowledge, the fabrication of lanthanide oxychloride thin films has thus far been restricted to chemical vapor deposition,[29,30] and the directed assembly of nanoscale oxychloride particles has not been previously reported. For many of the reasons outlined above, electrophoretic deposition of preformed nanoscale oxychloride particles represents a more practical alternative for the construction of phosphor displays, providing greater control over primary particle size and film texture and enabling conformal and high-throughput deposition at low temperatures as compared to vapor deposition techniques.

Although significant progress has now been achieved with the electrophoretic deposition of colloidal nanoparticles,[10−12,31,32] the deposited films are not typically characterized by a high degree of orientation or anisotropy, with a few notable exceptions. Sakka and co-workers have reported the electrophoretic deposition of oriented TiO_2 and α-Al_2O_3 particulate films with a high particle density by enlisting the assistance of a strong magnetic field in addition to the electric field that drives particle assembly.[33,34] Oriented nanostructured films of polydisperse anisotropic nanomaterials have also been reported by Ovtar et al. and Sugimoto et al. for $BaFe_{12}O_{19}$ platelets and tetratitanate nanosheets, respectively.[35,36] The former set of authors have posited that owing to their larger dimensions, the basal planes of anisotropic particles bear a higher net surface charge than the edges. Consequently, electrostatic interactions are strongest between the planar faces of nanoparticles and the electrode surface, assisting the growth of oriented deposits, although the polydispersity of the hydrothermally prepared platelets limits the extent of alignment within the deposits.[35,37] In the context of planar particles, Dickerson and co-workers and our research group have independently reported substantial alignment and control over the orientation of electrophoretically deposited thin films of single-layered graphene oxide.[38,39] As a particularly elegant example of the possibilities of this technique, Ahmed and Ryan have obtained vertically aligned arrays of CdS nanorods across large areas through electrophoretic deposition.[40] Here, we demonstrate that the electrophoretic deposition of monodisperse GdOCl nanoplatelets from stable colloidal dispersions in cyclohexane (colloidal stability being derived from surface-passivating ligands) permits a high degree of alignment to be obtained in the deposited thin films.

2. EXPERIMENTAL METHODS

Synthesis and Purification of GdOCl Nanoplatelets. GdOCl nanoplatelets with tri-*n*-octylphosphine oxide (TOPO) as the coordinating ligand were synthesized by the ligand exchange and condensation of gadolinium chloride and gadolinium isopropoxide through a modified nonhydrolytic sol−gel approach.[23,41,42] We have previously detailed the synthetic route and control over morphology possible through choice of the coordinating ligand.[23]

Preparation of Colloidal Dispersion of GdOCl Nanocrystals for Electrophoretic Deposition. Nonpolar colloidal dispersions of GdOCl nanoplatelets were prepared using cyclohexane as the dispersion medium. Varying dispersion concentrations (2.5, 5.0, 7.5, and 10.0 mg of GdOCl nanodisk powder dispersed in 10 mL of cyclohexane) were prepared to investigate the effects of nanocrystal concentration on the electrophoretic deposition process. Suspensions of GdOCl nanoplatelets in 2-propanol and water were also prepared at similar concentrations.

Electrophoretic Deposition of GdOCl Nanoplatelets. GdOCl nanoplatelets were deposited onto ITO-coated glass electrodes (Delta Technologies, sheet resistance R_s = 5−10 Ω/square; dimensions of ∼12.5 × 25 × 0.5 mm) from cyclohexane, 2-propanol, and aqueous dispersions by the application of a dc electric field. Conducting leads were attached to the two ITO electrodes by means of Ag-paste contacts. The voltage across the electrodes was applied using a Keithley 6517A high-resistance electrometer operated using a Labview 7.1 program. The ITO-coated glass substrates were arranged in a parallel-plate capacitor geometry with the conducting surfaces facing each other and a fixed ∼5 mm gap between the electrodes. The electrode assembly was fastened within the sample holder of a Tl0.01 dip coater (MTI Corp.). The electrode assemblies were then immersed into the GdOCl colloidal dispersions and dc electric fields were applied with the applied voltages ranging from 25−400 V (electric fields of 5000−80000 V/m) for varying times (1, 3, 5, 7, and 9 min). The suspensions were gently stirred in each instance to preclude sedimentation of the nanoplatelets. After deposition, the ITO electrodes with the deposited thin films were withdrawn from solution at a rate of 2 mm/min. The voltage was applied during the drying process to aid with densification of the coatings. Eddy currents and the evaporation of residual trapped solvent molecules are thought to be abetted by continuous application of a voltage over the duration of the drying process.[43]

Characterization. A JEOL 2010 transmission electron microscope (TEM) operated at an accelerating voltage of 200 kV was used to examine the GdOCl nanoplatelets and to obtain selected-area electron diffraction (SAED) patterns. To prepare the samples for HRTEM and SAED analysis, the nanoplatelets were dispersed in cyclohexane and then deposited onto 400-mesh carbon-coated Cu grids.

The ζ-potential, conductivity, and electrophoretic mobility of the colloidal GdOCl dispersions were measured using a Malvern Zetasizer Nano ZS90 instrument with excitation from a 632.8 nm He−Ne laser. A folded capillary cell was used for measurements of aqueous dispersions of GdOCl nanoplatelets, whereas dip cells were used for measurements in cyclohexane and 2-propanol. The Hückel approximation was used to calculate the ζ-potentials of the cyclohexane colloidal dispersions, whereas the Smoluchowski approximation was used to calculate the ζ-potentials for the water and 2-propanol dispersions.

Digital images of the film surfaces were obtained with an Olympus BX41 optical microscope. Uniformity and alignment of the obtained coatings were examined by scanning electron microscopy (SEM) using a Hitachi SU-70 scanning electron microscope operated at an accelerating voltage of 5 kV.

3. RESULTS AND DISCUSSION

Figure 1 shows electron microscopy images of the GdOCl nanoplatelets along with an indexed SAED pattern acquired for a single nanoplatelet indicating the single-crystalline nature of the particles. The high-resolution TEM image depicted in Figure 1A illustrates the (110) lattice planes on the basal plane of the nanoplatelets with a characteristic separation of 2.79 Å. GdOCl adopts a tetragonal matlockite PbFCl structure (space group: $P4/nmm$; $Z = 2$) with cationic layers of $(GdO)_n^{n+}$ and anionic layers of Cl^- alternating along the crystallographic c direction.[23] Figure 1C depicts a reconstruction of the GdOCl crystal structure when viewed down the crystallographic c direction depicting the (110) planes. Our synthetic method yields fairly monodisperse nanoplatelets with mean lateral dimensions of ~395 ± 10 nm. The SEM image in Figure 1D indicates the monodispersity of the nanoplatelets and also provides a cross-sectional view of their anisotropic morphology. Powder X-ray diffraction and Raman spectroscopy characterization of these materials have been previously published.[23]

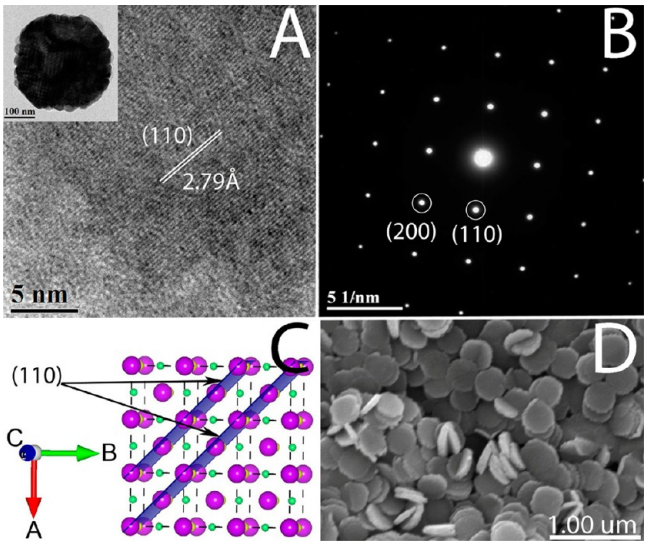

Figure 1. (A) High-resolution TEM image of an individual GdOCl nanoplatelet showing the separation between (110) lattice planes. The basal plane of the nanoplatelets corresponds to the *ab* plane. The inset shows a low-magnification image of the entire nanoplatelet. (B) SAED pattern acquired for a single GdOCl nanoplatelet. (C) View of the GdOCl unit cell (Gd atoms are depicted as the large purple spheres; O atoms are the smallest green spheres; and Cl atoms are depicted as yellow spheres) showing the (110) lattice planes corresponding to the view of the *ab* basal plane along the crystallographic *c* direction in (A). (D) High-magnification SEM image of GdOCl nanoplatelets.

Figure 2 plots the electrophoretic mobility (μ_e) distribution measured for the GdOCl nanoplatelets in cyclohexane, 2-propanol, and water for colloidal dispersions with a concentration of 500 mg/L. In cyclohexane (dielectric constant, $\varepsilon = 2.0$; viscosity, $\eta = 0.98$ cP), the magnitude of the electrophoretic mobility is the lowest and is centered around −0.09 μm·cm/V·s, which translates to an average ζ-potential of −66 mV. While the magnitude of the electrophoretic mobility and ζ-potential show some variability from batch to batch, the measured values are always negative in cyclohexane and the electrophoretic mobility tends to be smaller in magnitude than in the other two solvents. Based on Figure 2, while the majority of the GdOCl platelets are negatively charged in cyclohexane,

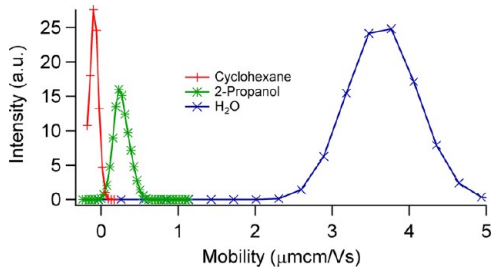

Figure 2. Electrophoretic mobility distributions of GdOCl nanoplatelets dispersed in cyclohexane, 2-propanol, and H_2O at a concentration of 500 mg/L.

the tail of the mobility distribution extends to positive values indicating a minority population of positively charged platelets. Using $\mu_e = Ze/(3\pi\eta d)$, where Z is the surface charge number (in units of charge e), and d is the hydrodynamic diameter,[1,31,44,45] we deduce from $\mu_e = -0.09$ μm·cm/V·s, $\eta = 0.98$ cP, and $d = 0.651$ μm, a Z value of $-0.54e$ (or 8.65×10^{-20} C) on average for a TOPO-capped GdOCl nanoplatelet in cyclohexane.

The surface charge of ligand-passivated colloidal nanocrystals has been variously attributed to thermal charging, undercoordinated surficial atoms, desorption of ionized ligands, charge transfer between the nanocrystals and the solvent, and adsorption of charged impurities.[16,31,45−47] For instance, populations of both positive and negatively charged colloidal particles are known to coexist in solution for CdSe quantum dots.[10,31,47] In the specific example under consideration, desorption of Gd—TOPO complexes from the nanoplatelet surfaces could lead to an uncompensated negative charge. Alternatively, phosphinic acid impurities in TOPO could be partly ionized at the particle interface giving rise to a negative charge. Also, it should be noted, that upon desorption, charged ligands are likely to remain in close vicinity of the colloidal nanoplatelets constituting part of the double layer surrounding the platelets and providing some extent of electrostatic stabilization.[14] Notwithstanding the positive tail evidenced in the mobility distribution, homogeneous deposition of nanoplatelet films has only been observed to proceed on the positive electrode upon application of a dc voltage (vide infra).

The electrophoretic mobility distributions are substantially modified (shifted entirely to positive values) and broadened upon dispersion of the GdOCl nanoplatelets in 2-propanol and water (Figure 2). The corresponding ζ-potential values in 2-propanol and water are +30 and +48 mV, respectively. Removal of additional ligands, solvent-polarity-dependent ligand ionization, and charge transfer can lead to the nanoplatelets possessing a broad range of surface charge states. Both galvanostatic and potentiostatic deposition of GdOCl nanoplatelet films are possible from 2-propanol and water solutions but the extent of particle alignment is substantially diminished in comparison to deposition from cyclohexane through the potentiostatic method. In contrast, presumably owing to the low conductivity of the cyclohexane dispersions, we have found it impossible to maintain uniform current densities in galvanostatic deposition mode. The resulting films tend to be patchy with limited reproducibility.

Figure 3 shows digital photographs and optical microscopy images of GdOCl nanoplatelet films electrophoretically deposited onto ITO-coated glass electrodes from cyclohexane dispersions at voltages ranging from 25−400 V (electric fields

dx.doi.org/10.1021/jp3051142 | J. Phys. Chem. B 2013, 117, 1585−1591

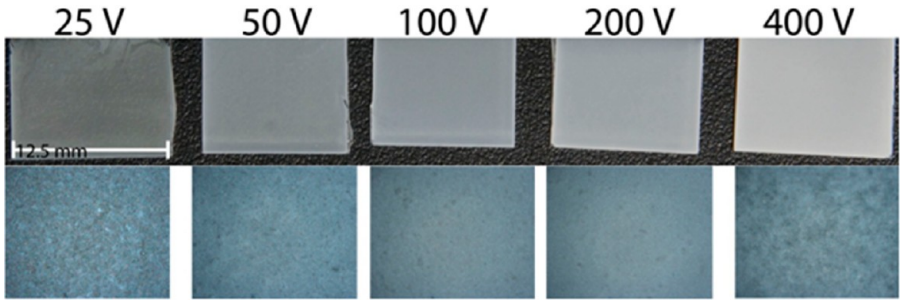

Figure 3. Top panels show digital photographs of GdOCl nanoplatelet films deposited onto ITO-coated glass electrodes at varying dc voltages ranging from 25−400 V for a period of 3 min. The lower panels show corresponding optical microscopy images depicting homogeneous coverage for the higher voltages.

of 5000−80000 V/m). A deposition time of 3 min and a solution concentration of 750 mg/L have been used in each instance. The films range from being transparent to completely opaque. Notably, no deposition of nanoplatelets has been observed in the absence of an electric field. The optical microscopy images indicate homogeneous, densely packed, and smooth films at higher voltages.

The SEM images in Figure 4 provide more detailed insight into mechanistic aspects of the deposition of oriented GdOCl nanoplatelet thin films. Figure 4A,B depicts the onset of nanoplatelet deposition (at the lowest concentration at which deposition is achieved, corresponding to 250 mg/L) upon the application of 25 V for 3 min and indicate the initially rather sparse coverage of predominantly individual nanoplatelets on the ITO surface. Clearly, individual nanoplatelets are deposited onto the positive electrodes, suggesting excellent colloidal stability (and absence of particle agglomeration) of the cyclohexane dispersions. It is evident that the particles are preferentially oriented such that their basal planes are aligned with the electrode surface. Figure 4C,D indicates a greater density of nanoplatelet coverage (albeit still submonolayer) when a more concentrated solution (500 mg/L) is used for electrophoretic deposition for the same period of time (3 min). Figure 4D suggests the preservation of a high degree of substrate alignment. Upon further increasing the concentration to 1000 mg/L, Figure 4E,F depicts multilayer coverage after electrophoretic deposition for 3 min, clearly showing the dense packing of the GdOCl nanoplatelets and the distinct preferential orientation of the deposited platelets such that their basal planes lie parallel to the ITO surface. Electrophoretic deposition in cyclohexane yields uniform and oriented deposits up to the concentrations of 1000 mg/L tested here (higher concentrations show visibly greater scattering and sedimentation indicative of decreased colloidal stability).

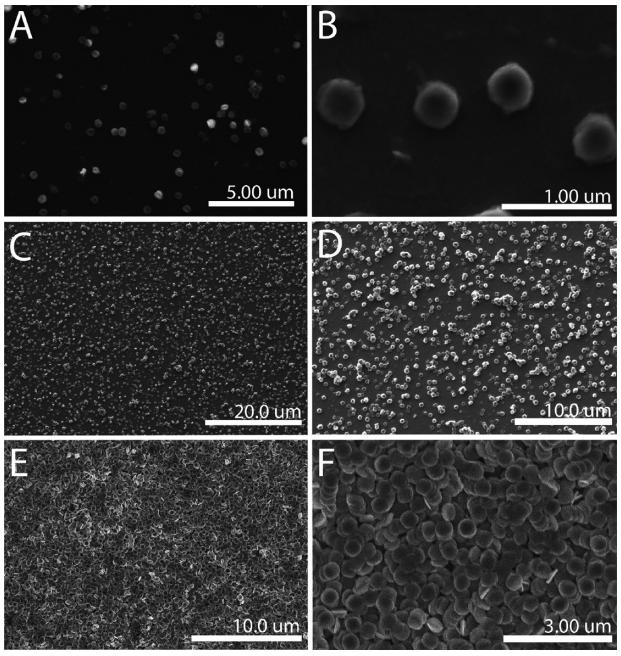

Figure 4. SEM images of GdOCl nanoplatelets deposited onto ITO-coated glass electrodes. (A) Electrophoretically deposited GdOCl nanoplatelets upon application of 25 V for 3 min. Deposition was performed using a 250 mg/L cyclohexane dispersion of the nanoplatelets. (B) A higher magnification view of (A). Both panels indicate the alignment of the planar faces of the nanoplatelets with the electrode surface. (C, D) Higher surface coverage is obtained upon deposition for 3 min using a 500 mg/L colloidal dispersion of the nanoplatelets. (E, F) Multilayer coverage with considerable retention of particle alignment is obtained upon deposition from a 1000 mg/L cyclohexane dispersion of the nanoplatelets. All films were deposited for 3 min.

Deposition can be continued over more prolonged durations (15 min) at 600 V to obtain oriented nanoplatelet films ranging up to several micrometers in thickness, whereby the nanoplatelets can almost entirely be depleted from solution. The micrometer-thick films can be readily delaminated from the ITO substrate to obtain macroscopic free-standing constructs ranging across several millimeters in size without need for a sacrificial layer. Figure 5 shows SEM images of fragments of free-standing GdOCl thin films. The inset to Figure 5A shows that the fragments can sustain substantial flexion without fracture, likely as a result of the flexible TOPO ligands passivating the nanoplatelets.[32,48]

The measured current decays rapidly during the electrophoretic deposition process as has been seen previously for other colloidal systems dissolved in nonpolar solvents.[10,45,49] In nonpolar solvents, the platelets are thought to be the primary charge carriers but counterions and other charged species are likely to exist in solution such as derived from partially ionized ligand molecules and ligand molecules that have desorbed while still being bonded to Gd cations. In a typical run, after deposition for 3 min at 25 V, the solution conductivity decreases from 3.74×10^{-4} ($\pm 8.9 \times 10^{-5}$) mS/cm to 1.9×10^{-4} ($\pm 3.5 \times 10^{-5}$) mS/cm. The ζ-potential distribution is also modified becoming more negative (centered at -41 ± 9 mV after deposition at 25 V compared to -16.8 ± 3 mV before deposition). The decrease in current likely also emanates from

dx.doi.org/10.1021/jp3051142 | J. Phys. Chem. B 2013, 117, 1585−1591

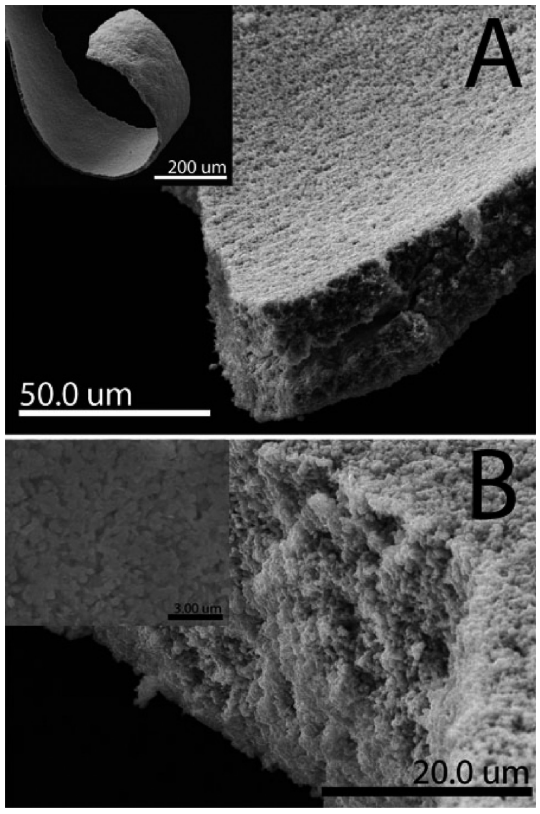

Figure 5. (A) SEM image of a fragments of a free-standing GdOCl nanoplatelet construct delaminated from the ITO-coated glass substrate. The thin films were originally deposited potentiostatically at 600 V for 15 min from 1000 mg/L cyclohexane dispersion. The inset shows the flexion of a free-standing fragment. (B) Cross-sectional SEM image of a free-standing fragment; the inset shows a top-view of the free-standing construct.

electrode polarization effects and the resistance drop across the incipient electrophoretically deposited film.[14]

Electrophoretic deposition under potentiostatic conditions involves two distinct processes. The first is the translational motion of the negatively charged GdOCl nanoplatelets to the positively charged electrode under the influence of the electric field as the applied electric field induces slip, relative motion, or separation, at the interface between the bulk cyclohexane medium and the platelet and its double layer up to the slip plane, the extent of the electric layer that accompanies the particle under direction of an electric field.[16] The viscous drag of the solvent and the counteracting repulsive force imposed by the electric field on oppositely charged counterions work in tandem to retard translation of the nanoplatelet and engender distortion of the double layer of a translating particle such that the frontal envelope of the double layer is thinned relative to the trailing section.[13,14] The second process involves deposition onto the electrode and involves charge transfer at the electrode or alternatively collapse of the platelet's electric double layer. For a negatively charged nanoplatelet approaching the anode under the influence of an applied field (with an already thinned double layer at the front), mobile positively charged ions in the diffuse layer can combine with negatively charged ions that have been attracted to the surface of the electrode (and have established a double layer at the electrode surface). The resulting neutral species are expected to diffuse to the bulk of the solution as per their concentration gradient. This is a possible mechanism for collapse of the double layer, which would enable the particle to adhere to the electrode surface and would further account for the decrease in conductivity of the solution. For nanoplatelets that do not "stick" to the electrode, the loss of counterions would be reflected in a higher negative charge, which would further account for the more negative ζ-potential observed after deposition.

The remarkable planar alignment of the GdOCl nanoplatelets and the establishment of high-particle-density packing motifs is further likely a function of the anisotropic charge distribution on the platelets as well as entrainment within electroosmotic flow adjacent to the electrodes.[50,51] For $BaFe_{12}O_{19}$ platelets, Ovtar et al. suggested that a higher net surface charge exists on the planar surfaces as compared to the edges and sides. As a result of this anisotropy in charge distribution, the platelets are subjected to an anisotropic electrophoretic force, which leads to preferential orientation on the electrode surface, thereby also maximizing van der Waals interactions between the particle and the surface.[35,52] The low electrophoretic mobility of GdOCl in cyclohexane (Figure 2) further permits individual nanoplatelets to orient in response to the applied electric field while translating through the cyclohexane medium. The SEM images in Figure 4A,B corroborate the contention of individual nanoparticles being deposited onto the electrodes.

Once the flux of particles reaches the electrode surface, Prieve et al. have shown that the establishment of a balance between the electrophoretic attractive force, double layer repulsion, and the kinetic energy of the particles (as well as gravity under the appropriate conditions) leads to Brownian motion that is not entirely random but is instead distributed along a defined electrode-particle separation.[50,53] In other words, the particles can be considered to be levitating above the electrode surface, wherein they distort the uniform electric field applied normal to the electrode, thereby giving rise to electroosmotic flow in their immediate vicinity. The predominant contribution to electroosmotic flow induced around the levitating particle comes from the interaction of the electric field with mobile ions in the diffuse layer of the particle, which has been deduced to be an order of magnitude higher than flow intensity induced under the particle as a result of perturbations of the applied electric field by the particle.[50,53] Electroosmotic flow patterns established in close proximity to the electrodes upon the approach of the electrophoretically attracted nanoplatelets lead to induction of a viscous stress, which can entrain the particles into closely packed and highly oriented assemblies, as evident in Figure 4E,F.

Good colloidal stabilization and relatively sluggish electrophoretic mobilities have been found to be imperative for the oriented deposition of the GdOCl nanoplatelets. Figure 6 shows SEM images of GdOCl nanoplatelets deposited potentiostatically from a 500 mg/L 2-propanol solution (ε = 20.2; η = 2.04) at voltages ranging from 25−100 V. Agglomerates are visible even for the lower deposition voltages and the platelets appear to be deposited rather inhomogeneously with a far diminished extent of substrate alignment as compared to deposition from cyclohexane. The thin films deposited from water dispersions are of considerably worse quality with extensive clumping of the nanoplatelets and patchy coverage of the electrode surface.

Figure 7 shows the GdOCl nanoplatelet films deposited under galvanostatic conditions at a constant current of 0.75 mA from a 1000 mg/L 2-propanol dispersion. While homogeneous

dx.doi.org/10.1021/jp3051142 | J. Phys. Chem. B 2013, 117, 1585−1591

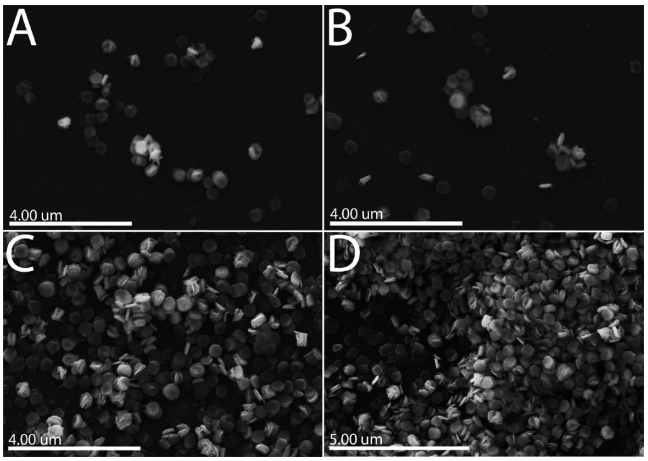

Figure 6. SEM images of GdOCl nanoplatelets deposited potentiostatically from a 500 mg/L 2-propanol colloidal dispersion at voltages of (A) 25, (B) 50, (C) 75, and (D) 100 V.

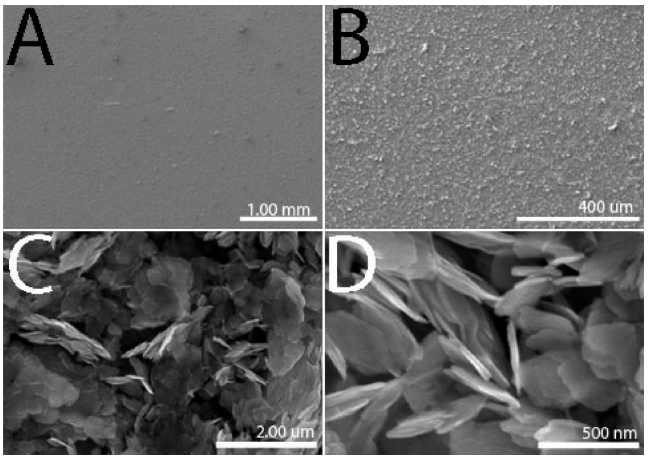

Figure 7. (A–D) SEM images of GdOCl films galvanostatically deposited onto ITO-coated glass electrodes from 2-propanol solution at a constant current of 0.75 mA.

coverage is obtained, the deposited films are much rougher and agglomeration of the nanoplatelets is discernible in the high-magnification SEM images shown in Figure 7C,D. The absence of substrate alignment for deposition from 2-propanol can be attributed to the relatively poor colloidal stability of TOPO-capped GdOCl nanoplatelets in this solvent, which leads to agglomeration in solution. Furthermore, the higher dielectric constant of 2-propanol and water results in a greater extent of Joule heating of the medium, which can potentially disrupt the equilibrium charge electroosmotic flows responsible for ordered entrainment of the nanoplatelets.[13,54] The measured electrophoretic mobilities are furthermore higher in 2-propanol and water (Figure 2), which likely leads to more rapid deposition (as compared to cyclohexane) under the same conditions. Entrainment within a higher flux of electrophoretically attracted incoming particles is expected to lead to complex flow lines and more disordered deposits.

As an illustration of the broad applicability of the electrophoretic deposition method for this class of materials, Figure 8 presents digital photographs of electrophoretically deposited thin films of Tb-doped GdOCl nanoplatelets with 2% Tb substitution on the cation sublattice. The synthesis of $Tb_{0.02}Gd_{0.98}OCl$ has been previously published.[23] Homogeneous green phosphorescent films are obtained with a high packing density of the constituent phosphor nanoplatelets.

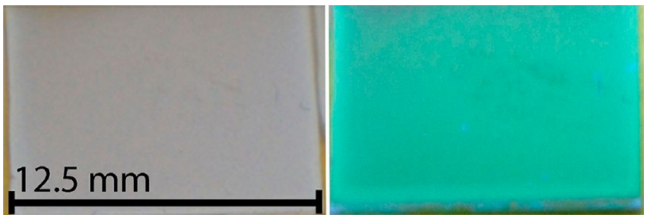

Figure 8. Digital photograph of a homogeneous $Tb_{0.02}Gd_{0.98}OCl$ nanoplatelet film deposited potentiostatically under 254 nm UV light illumination.

4. CONCLUSIONS

Electrophoretic deposition has emerged as a powerful enabling tool for nanoscience and nanotechnology, permitting the high-throughput assembly of nanostructured coatings and near-net-shape objects without requiring the addition of extraneous additives or complex surface modification. We demonstrate here the oriented electrophoretic deposition of TOPO-capped GdOCl nanoplatelets with a high degree of substrate alignment wherein the basal planes of the nanoplatelets reside parallel to the electrode surface. To the best of our knowledge, this represents the first example of oriented electrophoretic deposition of ligand-capped colloidal nanoparticles from a nonpolar solvent. The high substrate orientation and good packing of nanoplatelets arises from the anisotropic electrophoretic force to which they are subjected as a result of the anistropic charge distribution around the nanoplatelets as well as due to entrainment within electroosmotic flows established in proximity to the electrodes. The film thickness can be varied from submonolayer coverage to several tens of micrometers. The thicker films can be delaminated to obtain macroscopic free-standing nanoparticulate constructs. Future work will focus on more extensive characterization of phosphor quality for lanthanide-doped GdOCl nanoplatelet thin films.

AUTHOR INFORMATION

Corresponding Author

*Fax: 716-645-6963. E-mail: sb244@buffalo.edu.

Notes

The authors declare no competing financial interest.

ACKNOWLEDGMENTS

This work was supported by the National Science Foundation under DMR 0847169. The authors acknowledge Prof. Edward P. Furlani for helpful discussions.

REFERENCES

(1) Shevchenko, E. V.; Talapin, D. V.; Kotov, N. A; O'Brien, S.; Murray, C. B. *Nature* **2006**, *439*, 55–59.
(2) Dabbousi, B. O.; Murray, C. B.; Rubner, M. F.; Bawendi, M. G. *Chem. Mater.* **1994**, *6*, 216–219.
(3) Kim, F.; Kwan, S.; Akana, J.; Yang, P. *J. Am. Chem. Soc.* **2001**, *123*, 4360–4361.
(4) Mamedov, A. A.; Kotov, N. A. *Langmuir* **2000**, *16*, 5530–5533.
(5) Vendamme, R.; Onoue, S. Y.; Nakao, A.; Kunitake, T. *Nat. Mater.* **2006**, *5*, 494–501.
(6) Pang, J.; Xiong, S.; Jaeckel, F.; Sun, Z.; Dunphy, D.; Brinker, C. J. *J. Am. Chem. Soc.* **2008**, *130*, 3284–3285.
(7) Jiang, C.; Markutsya, S.; Pikus, Y.; Tsukruk, V. V. *Nat. Mater.* **2004**, *3*, 721–7288.

(8) Klajn, R.; Bishop, K. J. M.; Fialkowski, M.; Paszewski, M.; Campbell, C. J.; Gray, T. P.; Grzybowski, B. A. *Science* **2007**, *316*, 261−264.
(9) Podsiadlo, P.; Arruda, E. M.; Kheng, E.; Waas, A. M.; Lee, J.; Critchley, K.; Qin, M.; Chuang, E.; Kaushik, A. K.; Kim, H.; Qi, Y.; Noh, S.; Kotov, N. A. *ACS Nano* **2009**, *3*, 1564−1572.
(10) Islam, M. A.; Herman, I. P. *Appl. Phys. Lett.* **2002**, *80*, 3823.
(11) Mahajan, S. V.; Dickerson, J. H. *Nanotechnology* **2010**, *21*, 145704.
(12) Mahajan, S. V.; Dickerson, J. H. *Appl. Phys. Lett.* **2010**, *96*, 113105.
(13) Biest, O. O.; Van der; Vandeperre, L. J. *Annu. Rev. Mater. Sci.* **1999**, *29*, 327−352.
(14) Sarkar, P.; Nicholson, P. S. *J. Am. Ceram. Soc.* **1996**, *79*, 1987−2002.
(15) Hasan, S. A; Kavich, D. W.; Dickerson, J. H. *Chem. Commun.* **2009**, 3723−3725.
(16) *Electrophoretic Deposition of Nanomaterials*; Dickerson, J. H., Boccaccini, A. R., Eds.; Springer: New York, NY, 2012.
(17) Shane, M. J.; Talbot, J. B.; Schreiber, R. D.; Ross, C. L.; Sluzky, E.; Hesse, K. R. *J. Colloid Interface Sci.* **1994**, *165*, 325−333.
(18) Kitabatake, T.; Uchikoshi, T.; Munakata, F.; Sakka, Y.; Hirosaki, N. *J. Ceram. Soc. Jpn.* **2008**, *116*, 740−743.
(19) Russ, B. E. *J. Electrochem. Soc.* **1998**, *145*, 1253.
(20) Chang, D. C.; Talbot, J. B.; Rao, R. P.; Holland, C. *J. Soc. Inf. Disp.* **2000**, *8*, 51.
(21) Talbot, J. B. In *Electrophoretic Deposition of Phosphors for Information Displays and Solid State Lighting*; Dickerson, J. H., Boccaccini, A. R., Eds.; Springer: New York, NY, 2012; Ch. 7, pp 267−294.
(22) *Practical Applications of Phosphors*; Yen, W., Shionoya, S., Yamamoto, H., Eds.; CRC Press: New York, 2006.
(23) Kort, K. R.; Banerjee, S. *Inorg. Chem.* **2011**, *50*, 5539−5544.
(24) Uitert, L. G.; Van; Levinstein, H. J.; Grodkiewicz, W. H. *Mater. Res. Bull.* **1969**, *4*, 381−389.
(25) Rambabu, U.; Annapurna, K.; Balaji, T.; Buddhudu, S. *Mater. Lett.* **1995**, *23*, 143−146.
(26) Hölsä, J.; Lamminmäki, R. J.; Lastusaari, M.; Porcher, P. *J. Alloys Compd.* **2001**, *323*−*324*, 811−815.
(27) Konishi, T.; Shimizu, M.; Kameyama, Y.; Soga, K. *J. Mater. Sci.: Mater. Electron.* **2007**, *18*, 183−186.
(28) Li, G.; Li, C.; Zhang, C.; Cheng, Z.; Quan, Z.; Peng, C.; Lin, J. *J. Mater. Chem.* **2009**, *19*, 8936.
(29) Barreca, D.; Gasparotto, A.; Maragno, C.; Tondello, E.; Bontempi, E.; Depero, L. E.; Sada, C. *Chem. Vap. Deposition* **2005**, *11*, 426−432.
(30) Malandrino, G.; Perdicaro, L. M. S.; Fragalà, I. L. *Chem. Vap. Deposition* **2006**, *12*, 736−741.
(31) Jia, S.; Banerjee, S.; Herman, I. P. *J. Phys. Chem. C* **2008**, *112*, 162−171.
(32) Banerjee, S.; Jia, S.; Kim, D. I.; Robinson, R. D.; Kysar, J. W.; Bevk, J.; Herman, I. P. *Nano Lett.* **2006**, *6*, 175−80.
(33) Uchikoshi, T.; Suzuki, T. S.; Iimura, S.; Tang, F.; Sakka, Y. *J. Eur. Ceram. Soc.* **2006**, *26*, 559−563.
(34) Uchikoshi, T.; Suzuki, T. S.; Okuyama, H.; Sakka, Y.; Nicholson, P. S. *J. Eur. Ceram. Soc.* **2004**, *24*, 225−229.
(35) Ovtar, S.; Lisjak, D.; Drofenik, M. *J. Am. Ceram. Soc.* **2011**, *94*, 3373−3379.
(36) Sugimoto, W.; Terabayashi, O.; Murakami, Y.; Takasu, Y. *J. Mater. Chem.* **2002**, *12*, 3814−3818.
(37) Lisjak, D.; Ovtar, S. *Langmuir* **2011**, *27*, 14014−14024.
(38) Lee, V.; Whittaker, L.; Jaye, C.; Baroudi, K. M.; Fischer, D. A.; Banerjee, S. *Chem. Mater.* **2009**, *21*, 3905−3916.
(39) Hasan, S. A; Rigueur, J. L.; Harl, R. R.; Krejci, A. J.; Gonzalo-Juan, I.; Rogers, B. R.; Dickerson, J. H. *ACS Nano* **2010**, *4*, 7367−7372.
(40) Ahmed, S.; Ryan, K. M. *Chem. Commun.* **2009**, 6421−6423.
(41) Depner, S. W.; Kort, K. R.; Jaye, C.; Fischer, D. A.; Banerjee, S. *J. Phys. Chem. C* **2009**, *113*, 14126−14134.
(42) Depner, S. W.; Kort, K. R.; Banerjee, S. *CrystEngComm* **2009**, *11*, 841.
(43) Boccaccini, A.; Roether, J.; Thomas, B. *J. Ceram. Soc. Jpn.* **2006**, *14*, 1−14.
(44) Johnsson, M.; Edwards, K. *Biophys. J.* **2003**, *85*, 3839−3847.
(45) Hasan, S. A.; Kavich, D. W.; Mahajan, S. V.; Dickerson, J. H. *Thin Solid Films* **2009**, *517*, 2665−2669.
(46) Alivisatos, A. P. *J. Phys. Chem.* **1996**, *100*, 13226−13239.
(47) Islam, M. A. *Nanotechnology* **2008**, *19*, 255708.
(48) Jia, S.; Banerjee, S.; Lee, D.; Bevk, J.; Kysar, J. W.; Herman, I. P. *J. Appl. Phys.* **2009**, *105*, 103513.
(49) Islam, M. A.; Xia, Y.; Steigerwald, M. L.; Yin, M.; Liu, Z.; O'Brien, S.; Levicky, R.; Herman, I. P. *Nano Lett.* **2003**, *3*, 1603−1606.
(50) Prieve, D. C.; Sides, P. J.; Wirth, C. L. *Curr. Opin. Colloid Interface Sci.* **2010**, *15*, 160−174.
(51) Solomentsev, Y.; Böhmer, M.; Anderson, J. L. *Langmuir* **1997**, *13*, 6058−6068.
(52) Ohshima, H. *J. Colloid Interface Sci.* **1997**, *185*, 131−139.
(53) Sides, P. J.; Wirth, C. L.; Prieve, D. C. In *Mechanisms of Directed Assembly of Colloidal Particles in Two Dimensions by Application of Electric Fields*; Dickerson, J. H., Boccaccini, A. R., Eds.; Springer: New York, NY, 2012; Ch. 1, pp 3−72.
(54) Kornbrekke, R. E.; Morrison, I. D.; Oja, T. *Langmuir* **1992**, *8*, 1211−1217.